This is the accepted version of the following article:

Fraenkl, M., Frumarova, B., Podzemna, V., Slang, S., Benes, L., Vlcek, M., &Wagner, T. (2018). How silver influences the structure and physical properties of chalcogenide glass $(GeS_2)_{50}(Sb_2S_3)_{50}$. *Journal of Non-Crystalline Solids*, 499, pp. 412-419. doi: 10.1016/j.jnoncrysol.2018.07.046

This postprint version is available from URI https://dk.upce.cz//handle/10195/72629

Publisher's version is available from

https://www.sciencedirect.com/science/article/pii/S0022309318304447?via%3Dihub

This postprint version is licenced under a Creative Commons Attribution-NonCommercial-NoDerivatives 4.0.International.

How silver influences the structure and physical properties of chalcogenide glass $(GeS_2)_{50}(Sb_2S_3)_{50}$

Max Fraenkl[1,*], Bozena Frumarova[2], Veronika Podzemna[3], Stanislav Slang[3], Ludvik Benes[1], Milan Vlček[2], Tomas Wagner[1,3]

[1] *Department of General and Inorganic Chemistry University of Pardubice, Studentska 95,53210 Pardubice, Czech Republic*
[2]*Institute of Macromolecular Chemistry AS CR, v.v.i., Heyrovsky sq. 2, 162 06 Prague, Czech Republic*
[3]*Center of Materials and Nanotechnologies, Faculty of Chemical Technology, University of Pardubice, Studentska 95, 532 10 Pardubice, Czech Republic*

[*]corresponding author: Max Fraenkl, tel.: +420 725 572, email: max.fraenkl@student.upce.cz

Abstract

The presented study shows how the incorporation of silver changes the structure and physical properties of chalcogenide glass $(GeS_2)_{50}(Sb_2S_3)_{50}$. Nine samples with silver content (0-25 at. %) were studied to give a detailed picture. The structure and its changes were analyzed by Raman spectroscopy. The main structural units of the $(GeS_2)_{50}(Sb_2S_3)_{50}$ glass and its medium range order were described. Interaction of silver and hosting $(GeS_2)_{50}(Sb_2S_3)_{50}$ matrix was described by a set of chemical reactions. The weakest part of the hosting matrix, two interconnected $SbS_{3/2}$ pyramids, was identified. Such structural motif was identified as the doorway for silver incorporation. The material hardness is significantly increased by up to 26% due to silver addition. The ability of silver to fill cavities in a glass is responsible for the observed hardness increase. Electronic properties and silver ion mobility were examined by impedance spectroscopy and radioactive tracer diffusion. The purpose of the presented study is to give an instructive description of how silver change the structure of the studied chalcogenide glass and give a complex feeling of how the silver changes its physical properties.

Keywords: silver doping, chalcogenide glasses, hardness, impedance spectroscopy, radioactive tracer diffusion

1. Introduction

Silver doped chalcogenide glasses compared to undoped chalcogenide glasses exhibit red-shifted absorption, higher index of refraction and steep increase in electrical conductivity. Introduced silver into chalcogenide glass became cation Ag^+. The charge of the Ag^+ cation is compensated by C_1^-(one-fold coordinated chalcogen) [1, 2] . The silver doped chalcogenide glasses, with Ag concentration higher than ≈ 5 at.%, are a good ionic conductor [3]. Increase of the electrical conductivity could reach up to 11 orders of magnitude (from 0 to 30 at.% of Ag) [4].The good ionic conductivity and ability of silver to form a conductive filament make silver doped chalcogenide glasses a good candidate for a Conductive Bridge RAM memory. The Conductive Bridge RAM memory is today one of the most promising applications of silver doped chalcogenide glasses with an industrial significance[5]. The $(GeS_2)_y(Sb_2S_3)_{1-y}$ glasses belong among the important pseudo-binary chalcogenides. These glasses are attractive for silver doping because of two main reasons : 1) the $(GeS_2)_y(Sb_2S_3)_{1-y}$ glasses are well described, as they were object of numerous studies regarding glassforming properties [6], structural properties [7-10], optical properties [11], and mechanical properties[12]; and 2) the silver doping of ternary GeSbS glasses has not yet been studied in detail. The aim of the present work is to describe how silver influences the structure and the physical properties of the chalcogenide bulk glass $(GeS_2)_{50}(Sb_2S_3)_{50}$. The structural changes, hardness evolution and electronic / ionic properties are of the special interest.

2. Experimental

2.1. Glass preparation

The samples $Ag_x((GeS_2)_{50}(Sb_2S_3)_{50})_{1-x}$ glasses where x = 0, 0.1, 1, 5, 7.5, 10, 12.5, 15, 17.5, 20, and 25 were prepared. Appropriate amount of elements (Ge, Sb, S, Ag) of 5N purity was sealed into evacuated silica ampule. Each batch has about 10 g. Synthesis was done in a rocking furnace at temperature 970 °C for 36 hours. Then the samples were quenched from temperature 700 °C into the water and annealed for 3 hours ca. 20 °C under Tg. Composition and glass homogeneity was tested by SEM microscope Lyra 3 (Tescan) equipped with EDX analyser AZtec X-Max 20 (Oxford Instruments), and Bruker AXS diffractometer D8. The DSC measurements were performed using Q2000 heat-flow calorimeter (TA Instruments). Microhardness was measured by Hanemann's microhardness-meter with Vickers' pyramid, supplied with a Zeiss-Neophot microscope. Density of samples was measured by Archimedes method.

2.2. Raman spectroscopy

Raman scattering spectra were measured by Dimension P2 system (Lambda Solution, USA) Spectra were excited with a laser operating at 532 nm (output power 5 mW). Reduced Raman intensity of glasses Raman spectra were calculated considering the Gammon–Shuker equation [13]

2.3. Microhardness

Microhardness was measured by Vickers method. There was applied a load of 80 g for 10 seconds. The six measurements were done for each sample.

2.4. Electrical conductivity measurement

The dimension of each bulk sample was about 5x5 mm and thickness about 1 mm. The both sides were polished and Pt sputtered. Impedance spectroscopy measurement was performed

by impedance spectrometer Autolab PGSTAT204 in frequency range 10 mHz – 100 kHz from 20 °C up to 150 °C. The sample of $Ag_{15}((GeS_2)_{50}(Sb_2S_3)_{50})_{85}$ composition was measured at Alpha-A Analyser from Novocontrol and at Keysight E4991B Impedance Analyser (at higher frequencies).

2.5. Radioactive tracer diffusion measurement

Radioactive tracer diffusion (RTD) measurement was performed at three glass composition $Ag_x((GeS_2)_{50}(Sb_2S_3)_{50})_{1-x}$ where x=0, 7.5, and 15. Seven samples were prepared from each composition. A drop of radioactive $^{110m}AgNO_3$ was deposited on top of sample. The drop was kept for a certain period and dried. The samples, containing radioactive silver on their surface, were encapsulated into the ampules and annealed at different temperatures from a couple of hours to a couple of days. The penetration profile of silver inside annealed samples was evaluated by a multistep process. As first, the total gama activity was measured by scintillation counter. After that, a few units of microns from top of the samples were grinded. The both steps were repeated ca. 8 times.

3. Results

3.1.General

The prepared sample without silver $(GeS_2)_{50}(Sb_2S_3)_{50}$ has a red colour but with an increasing content of silver the samples became gradually darker and metallic shiny. The density of the samples increases proportionally to the content of silver as shown in Fig. 1. The value of glass-transition temperature T_g declines steeply for small concentration $x < 5$, then decrease

slowly as shown in Fig. 1. XRD and SEM microscopy prove that samples are glassy where silver concentration $x \leq 15$. The samples are glassy with crystalline inclusions for $x \geq 17.5$. The crystalline inclusions are separated by a glassy phase and represent a minor portion (ca. 5 %) of the whole sample (Fig. 2.). XRD results show that crystals are antimony for samples x = 17.5, 20, and 25 at. % and argyrodite [14] Ag_8GeS_6 for sample x = 25. The corresponding crystallization patterns are shown in the previous work [15]. The antimony crystals are rhombohedral (R3m – 166) – the lattice parameters were: a = 4.3105 Å, c = 5.6404 Å. The argyrodite (Ag_8GeS_6) crystals are orthorhombic (Pna21–33) – the lattice parameters were a = 15.149 Å, b = 7.476 Å, c = 10.589 Å. The antimony crystals in samples with x = 20, 25 have a needle like shape (Fig. 1e). Their pattern was revealed after a wet etch in NaOH solution. The sample where x = 25 was phase separated into micro and macro levels. SEM microscopy reveals the microscopic spheres, ca. 3 microns in diameter (Fig. 2 d,f). As well macroscopical sphere of diameter ca. 6 mm was found. The composition of the metallic like sphere was 80 at. % Sb, and 20 at. % Ag. The XRD measurement of the macroscopic sphere reveals, the Sb crystals rhombohedral (R3m – 166) – the lattice parameters were: a = 4.3105 Å, c = 5.6404 Å, and dyscrasite Ag_3Sb crystals orthorhombic (Pmnm 59) – the lattice parameters were: a = 5.9900 Å, b = 5.2400 Å, c = 4.8500. The macroscopic sphere decreases the content of the Sb by 10 % and Ag by 3 % in the glassy part of the sample as was proved by EDX measurement. The phase separation of the sample where x = 25 affects the density and impedance measurement as shown in the Figures (1) and (6). EDX analysis of studied samples (x = 0 - 20) confirmed that their overall composition is close to the nominal values.

3.2.Structural changes observed by Raman spectroscopy

Raman spectra of the studied hosting matrix $(GeS_2)_{50}(Sb_2S_3)_{50}$ are in good agreement with Raman spectra of the similar glasses of Ge-Sb-S system [6, 7, 16-18]. All the data were scaled by area and decomposed in a series of Raman peaks. (Fig. 3).

The Raman band between 200 and 450 cm^{-1} can be decomposed into 7 bands with maxima near 250, 283, 318, 340, 360, 388 and 414 cm^{-1}. The three main Raman bands, located at 340, 318 and 283 cm^{-1}, have been attributed to symmetric stretching vibrations of corner- sharing $GeS_{4/2}$ tetrahedra and to asymmetric and symmetric stretching vibrations of $SbS_{3/2}$ pyramids. The smaller bands at 360, 388 and 414 cm^{-1} can be ascribed to the edge-shared $GeS_{4/2}$ tetrahedral symmetric stretching vibrations, to asymmetric stretching vibrations of corner-shared $GeS_{4/2}$ tetrahedra and bridging sulfur vibrations in the $S_3Ge\text{-}S\text{-}GeS_3$ structural units, respectively. The band 250 cm^{-1} can be assigned to vibrations of Ge-Ge bonds in $S_3Ge\text{-}GeS_3$ ethane-like structural units. The broad band of low intensity in the region 100 – 200 cm^{-1} can be decomposed into 2 bands at 150 and 170 cm^{-1} corresponding to asymmetric bending vibrations of $GeS_{4/2}$ and Sb-Sb vibrations in units $S_2Sb\text{-}SbS_2$.

The changes of the bands in Raman spectra induced by silver incorporation could be separated into two regions (1 and 2) according to silver concentration in the sample:

1) Silver concentration (0.1 – 15 at. %)

There main Raman bands: symmetrical vibration $SbS_{3/2}$ (283 cm^{-1}), asymmetrical vibration of $SbS_{3/2}$ (318 cm^{-1}), vibration of corner-sharing (CS) $GeS_{4/2}$ tetrahedra (340 cm^{-1}), decreases its intensity due to the interaction with silver. Those three bands were called “REACTANTS” (Fig. 4a).It is worthy to note, that the band of symmetrical vibration $SbS_{3/2}$ (283 cm^{-1}) decreases quasi proportionally while silver concentration increases in the sample. Two Raman bands with a homopolar bond: $S_2Sb\text{-}SbS_2$ (170 cm^{-1}), and ethane-like unit $S_3Ge\text{-}GeS_3$ (250 cm^{-1}) increase their intensity with the increasing content of silver. Those two bands were

called “PRODUCTS”.(Fig. 4b). The first silver addition generates band at 212cm^{-1}, such a band was found in Raman spectra of thin film Ag_2S [19]. As well the presence of (pyro-($GeS^{3-}_{3.5}$), meta-(GeS^{2-}_{3}), di-($GeS^{1-}_{2.5}$) thiogermanate tetrahedra was identified [20-22]. These structures are evidence of the presence of non-bridging sulphur.

2) Silver concentration (17.5 - 25 at. %)

An important change in the structure takes place when silver concentration in the sample reaches 17.5 at. %. The small part of antimony crystalizes. Antimony in the crystalline phase is presented in samples with concentration of silver (17.5 - 25 at. %). In Fig. 4a,b it is visible, that amount of “REACTANTS” and “PRODUCTS” when $x \geq 17.5$ maintain roughly same level. There is only one significant change, the drop of the signal of S_2Sb-SbS_2 (170 cm^{-1}).

3.3.Microhardness

Microhardness of the studied material increases with the increasing content of silver. Microhardness maximum is reached at silver concentration x = 17.5. After that, a significant drop of microhardness is observed. The maximal value of microhardness is higher by 26 % than the initial value of microhardness for x = 0 (Fig. 5). Each imprint of a diamond indentor shows the presence of cracks in each corner. Quality, of size measurement of the indentor imprint, was increased by using SEM microscopy (regarding to high quality optical microscopy). The result of sample microhardness for sample where x = 0 is in very good agreement with literature [12].

3.4.Electrical properties

The impedance spectroscopy measurement shows that DC conductivity of samples (x = 1 - 20) increases exponentially (Fig. 6a). The sample x = 0 was not measured because of very

low conductivity. Activation energy of DC electric conductivity decreases linearly (Fig. 6b). The measured impedance spectra follows the Time Temperature Superposition [23]. Impedance spectra of all samples were fitted (Fig. 7) by using a combination of two contributions shown in Eqs. (1 - 3). The first one is Dyre's model that describes ionic transport under a random distribution of potential barrier [24]. The complex conductivity $\sigma^*(\omega)$ is given as

$$\sigma^*(\omega) = \sigma(0)\frac{i\omega\tau_{max}}{\ln(1+i\omega\tau_{max})} \qquad (1)$$

where $\sigma(0)$ is the DC conductivity, τ_{max} is maximum hoping relaxation time and ω is the angular frequency. The second contribution describes a polarization of blocking electrodes, an effect that accompanies ionic conductivity at "lower" frequencies [25]. Overall complex conductivity $\sigma^*(\omega)$ is given by a summation of bulk and interfacial responses

$$\frac{1}{\sigma^*(\omega)} = \frac{1-f}{\sigma^*_{bulk}(\omega)} + \frac{f}{\sigma^*_{interface}(\omega)} \qquad (2)$$

where the bulk conductivity represents $\sigma^*_{bulk}(\omega)$ and the interfacial conductivity $\sigma^*_{interface}(\omega)$.The symbol *f* is the spectral weight of interfacial conductivity. The bulk complex conductivity is $\sigma^*_{bulk}(\omega) = \sigma_{b1} + i\sigma_{b2}$ and the complex interfacial conductivity $\sigma^*_{interface}(\omega) = \sigma_{i1} + i\sigma_{i2}$. Substituting the values of $\sigma^*_{bulk}(\omega)$ and $\sigma^*_{interface}(\omega)$ in above equation, we obtain

$$\frac{1}{\sigma^*(\omega)} = \frac{1-f}{\sigma_{b1}+i\sigma_{b2}} + \frac{f}{\sigma_{i1}+i\sigma_{i2}} \qquad (3)$$

where the subscribts *b* and *i* represents the interfacial and bulk regions, respectively.

3.5.Radioactive tracer diffusion experiment

The results of the radioactive tracer diffusion RTD experiment for samples where x = 0, 7.5 , and 15 are presented in Fig. 8. The measured RTD coefficients D_{tracer} were compared to calculated ones D_σ via Nernst-Einstein relation

$$D_\sigma = \frac{\sigma_i kT}{N(Ze)^2} \qquad (4)$$

where σ_i is the ionic conductivity obtained by impedance measurement. *N* is the number of mobile ions, *Z* is the ion charge, *e* is the charge of electron, *k* is the Boltzmann constant and *T* is the absolute temperature. The number of mobile ions is calculated based on assumption that all introduced silver became silver ions. The calculated and measured RTD coefficients are close together, but their curves have different slopes and hence different activation energies (Tab.1). The diffusion coefficient for the sample without silver could be evaluated only in case of the RTD experiment. The silver that diffuses in the sample where x = 0 is the one which is added artificially on top of sample in a drop of $^{110m}AgNO_3$ (see section 2.5).

The Haven ratio H_R was calculated using equation (5) [26, 27].

$$H_R = \frac{D_{tracer}}{D_\sigma} \qquad (5)$$

The results are presented in Tab. 1. The calculated *Hr* gives more than one value. The *Hr* is in our case dependent on the temperature, because of the different slopes of the measured D_{tracer} and the calculated D_σ diffusions coefficients as shown in Fig. 8 and Table 1.

4. Discussion

4.1.Understanding of the structural changes based on Raman spectroscopy

Our aim is to understand the way of silver incorporation into the hosting matrix $(GeS_2)_{50}(Sb_2S_3)_{50}$. It is vital, first of all, to know how the hosting matrix is built and which kind of information can Raman spectroscopy provide. In the first section (4.1.1.) the structure

and the medium range order of the system $(GeS_2)_y(Sb_2S_3)_{1-y}$ is described. The same approach will be applied in the second section (4.1.2.) to describe the glass $(GeS_2)_{50}(Sb_2S_3)_{50}$. The third section (4.1.3.) describes the object of this study, silver incorporation in the hosting matrix $(GeS_2)_{50}(Sb_2S_3)_{50}$.

4.1.1. Structure of $(GeS_2)_y(Sb_2S_3)_{1-y}$

Now we try to explain, based on the previous studies, how Raman spectroscopy helps to describe the structure of system $(GeS_2)_y(Sb_2S_3)_{1-y}$.The same approach will be used in the next section to describe our studied glass $(GeS_2)_{50}(Sb_2S_3)_{50}$. Lin et al. made an important analysis of the structure of the system $(GeS_2)_y(Sb_2S_3)_{1-y}$ [7]. They were able to describe the structure and medium range order of that system. They explained why the Raman signal corresponding to ES and CS $GeS_{4/2}$ tetrahedra vanishes once $y \leq 60$. The situation when $y = 60$, is for the system $(GeS_2)_y(Sb_2S_3)_{1-y}$ a compositional threshold. This is the state when each $GeS_{4/2}$ tetrahedra could be separated by the $SbS_{3/2}$ pyramid (ratio is 3:4). Once there is in the system, a sufficient amount of Sb_2S_3 pyramids ($y \leq 60$) they separate $GeS_{4/2}$ tetrahedra. It is a moment when the Raman signal of ES and CS $GeS_{4/2}$ vanishes. There is an obvious strong tendency of Sb_2S_3 pyramids to separate the $GeS_{4/2}$ tetrahedra. The medium range order is proposed, based on that finding, in the case of the system $(GeS_2)_y(Sb_2S_3)_{1-y}$ [7]. Because there are no figures showing integrated intensities of Raman signal of $(GeS_2)_y(Sb_2S_3)_{1-y}$ in the work of Lin et al. we would like to use results presented in work of R. Svoboda et al.(Fig. 9) [9]. In Fig. 9, it is visible that the signal of CS $GeS_{4/2}$ tetrahedras is decreasing with increasing content of Sb_2S_3. The signal of CS $GeS_{4/2}$ tetrahedras tends to minimize once the compositional threshold is reached ($y < 60$). This is the confirmation that Sb_2S_3 pyramids separate $GeS_{4/2}$ tetrahedras.This information will be used in the next section to describe the structure of the studied hosting matrix $(GeS_2)_{50}(Sb_2S_3)_{50}$. We can also get quantitative information from Raman spectroscopy of studied glass $(GeS_2)_y(Sb_2S_3)_{1-y}$. We found in the work of R. Svoboda

et al. [9], that there is one Raman signal which is proportional to y. The signal is a symmetrical vibration of the $SbS_{3/2}$ pyramid (190 cm^{-1}) which is proportional to the content of Sb_2S_3 (Fig. 9). There is no information about content of $GeS_{4/2}$ itself, only about two interconnected units of CS or ES $GeS_{4/2}$.

4.1.2. Structure of $(GeS_2)_{50}(Sb_2S_3)_{50}$

Now we describe the glass $(GeS_2)_{50}(Sb_2S_3)_{50}$, which is the hosting matrix for silver incorporation. Such a glass has excess of $SbS_{3/2}$ pyramids compared to $GeS_{4/2}$ tetrahedras. Once we follow the rule mentioned above, that $SbS_{3/2}$ pyramid tends to separate $GeS_{4/2}$ tetrahedras, we can find by a simple combination [8], that the glassy matrix $(GeS_2)_{50}(Sb_2S_3)_{50}$ is organised in that way:

1/3 of $SbS_{3/2}$ pyramids have neighbours : 3 $GeS_{4/2}$ tetrahedras

1/3 of $SbS_{3/2}$ pyramids have neighbours : 2 $GeS_{4/2}$ tetrahedras and 1 $SbS_{3/2}$ pyramid

1/3 of $SbS_{3/2}$ pyramids have neighbours: 1 $GeS_{4/2}$ tetrahedra and 2 $SbS_{3/2}$ pyramids

In the hosting matrix $(GeS_2)_{50}(Sb_2S_3)_{50}$ there will be 80 % of $SbS_{3/2}$ pyramid – $GeS_{4/2}$ tetrahedra connections and 20 % of $SbS_{3/2}$ - $SbS_{3/2}$ pyramid connections. However, this is an ideal description of hosting matrix $(GeS_2)_{50}(Sb_2S_3)_{50}$. Results of our study and also Fig. 9 show that there is small quantity of CS $GeS_{4/2}$ tetrahedras which remain even for $y < 60$.

4.1.3. Silver incorporation in $(GeS_2)_{50}(Sb_2S_3)_{50}$

We propose 4 main chemical reactions of silver with the hosting matrix $(GeS_2)_{50}(Sb_2S_3)_{50}$ (1-4), which include stoichiometric coefficients.

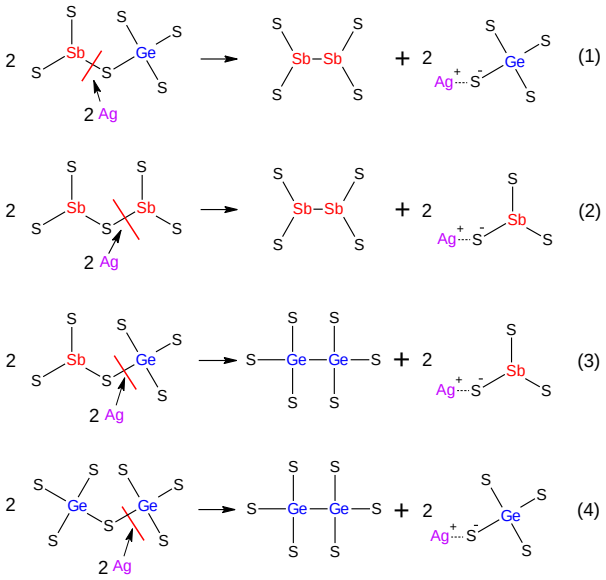

We drew, for better comprehensibility, that silver is “attacking” some existing position in the structure (1-4). In fact silver presence prevents these parts of the glassy matrix to be built. The products of reactions are $S_2Sb\text{-}SbS_2$, ethanlike $S_3Ge\text{-}GeS_3$ and non-bridging sulphur with silver cation. Reactions (1,2) are responsible for the decrease of Raman signal sym. $SbS_{3/2}$ pyramid (283 cm^{-1}), and reaction (4) is responsible for the decrease of signal CS $GeS_{4/2}$ tetrahedra (340 cm^{-1}) (Fig. 4a).

Further, a possible explanation, which one of reaction (1-4) is preferred and why, is given. The interconnection of $SbS_{3/2}$ pyramid and $GeS_{4/2}$ is in hosting matrix more preferred (section 4.1.1) and thus expected to be stronger. We suggest that the connection of two units $SbS_{3/2}$ and connection of two units $GeS_{4/2}$ is weak therefor the reaction (2) and (4) are favoured ones. To distinguish which one of the reactions (2) or (4) is preferred, we can rely on two findings. Firstly, the binding energy of Sb-S (260 kJ/mol) is lower than Ge-S (265 kJ/mol) [28]. Secondly, the study of the system GeSbS poor in chalcogen shows that the formation of Ge-S bonds is enhanced at the expense of Sb-S bonds[29]. Then we can decide that reaction (2), where the silver presence cuts the Sb-S bond (or more precisely silver prevents this bond from being created) will be the preferred one. Based on these findings we assume that the two

interconnected pyramids $SbS_{3/2}$ in reaction (2) are the doorway for silver incorporation in the glass $(GeS_2)_{50}(Sb_2S_3)_{50}$.

The antimony crystallization takes place once the content of silver is higher than 15 at. %. We can see in Raman spectra that amount of "REACTANTS" and "PRODUCTS" does not change, only the content of $S_2Sb\text{-}SbS_2$ (170 cm^{-1}) drops (Fig. 4b). We propose, that starts conversion (5) take place. This reaction consumes the structure $S_2Sb\text{-}SbS_2$ and produces the antimony.

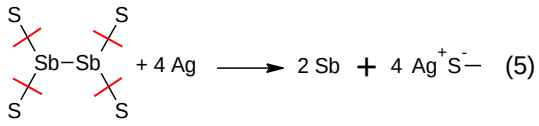

The last question is why reaction (2) does not continue and is replaced by reaction (5), although there is still ca. 70 % $SbS_{3/2}$ left (Fig. 4a)? A possible explanation could be that the reactant (interconnected pyramids $SbS_{3/2}$) is depleted. In the hosting matrix $(GeS_2)_{50}(Sb_2S_3)_{50}$ there is only 20 % of connection represented by two interconnected $SbS_{3/2}$ pyramids, as mentioned before in section 4.1.2.

4.2.Microhardness

The microhardness of studied samples increases with the increasing content of silver until concentration of silver reaches 17.5 at.% as shown in Fig. 5. There are two interesting facts related to that change. First one is that hardness increases while T_g is decreasing (Fig. 1). This is opposite to the empirical finding, that T_g is proportional to hardness of a material [30-32]. This rule is probably valid in the case of the glasses with covalent bonding character. The present system has a mixture of covalent and ionic bonds. Second one is the observation which relates to hardness and chemical bonding strength. Hardness of material is directly connected to the bonding strength between the atoms of a material. We do know that silver cuts and terminates structural chains by producing non-bridging sulphur with silver cation $-S^-$

Ag^+ (section 4.) Silver addition is responsible for reducing the content of strong Ge-S (265 kJ/mol) and Sb-S (260 kJ/mol) bonds in favour of newly created weak homopolar bonds Ge-Ge (185 kJ/mol) and Sb-Sb (175 kJ/mol) [28].

The silver itself is incorporated in the structure at the end of the structural backbone, and is bonded to the one sulphur by an ionic bond (Fig. 10). Silver in such a situation does not contribute to increase of glass network connectivity and thus to hardness increase.
Now we know that hardness increase does not originate in the increasing of the bonding strength and glass network connectivity. The position, which silver occupies in the hosting matrix, is probably responsible for the hardness increase. The density functional / molecular dynamics simulation performed by Akola et. al, shows that in, chalcogenide glasses $Ge_{0.42}S_{0.58}$ and AsS_2 are cavities that occupy ≈40 % of the total glass volume [33, 34]. Once silver is added in a concentration of 20 resp. 25 at.% the volume of cavities drops to ≈5 % of the total glass volume. The silver fills the cavities. The explanation why glass without silver has lower hardness could be found in fact that empty cavities collapse easily, once the external force is applied. When the silver is added the cavities are filled it prevents them from collapsing. The silver acts like a filling of the glassy structure. This is the way how the silver increases the hardness of the studied glass.

To demonstrate that the increase of hardness by 26 % from x = 0 to x = 17.5 (Fig. 5) is significant, we would like to compare our results with system $(GeS_2)_y(Sb_2S_3)_{1-y}$. The hardness in such a system increases with increasing content of GeS_2. But the hardness increases only by 17 % once content of GeS_2 increase from y = 0.2 to y = 0.9 [12]. We speculate that the sudden drop of hardness for the silver content exceeding 17.5 at% could be associated with appearance of crystalline phase of antimony, see Fig.2 [35].

4.3.Electrical properties of $Ag_x((GeS_2)_{50}(Sb_2S_3)_{50})_{1-x}$

DC conductivity of $Ag_x((GeS_2)_{50}(Sb_2S_3)_{50})_{1-x}$ samples increases by 8 orders of magnitude from $5x10^{-14}$ S/cm (x = 0.1) to $4.9x10^{-6}$ S/cm for x = 25. The increase of the DC conductivity is exponential for $1 \leq x \leq 20$. The character of electric conductivity is ionic as seen from the pronounced effect of electrode polarization (Fig. 7) and from the comparison of diffusion coefficients (Fig. 8). Increase of the DC conductivity with increasing silver content is smooth without a sudden change as was observed in other silver doped chalcogenides. This proves indirectly that the glassy matrix $(GeS_2)_{50}(Sb_2S_3)_{50}$ does not tend to be phase separated in the silver rich and silver poor phase [36, 37]. From the fact that, the DC conductivity does not change its exponential character when antimony crystals occur (x = 17.5) we can deduce that the antimony crystals (Fig. 2e) are not interconnected. Antimony has a high electrical conductivity ($2.4x10^4$ $S.cm^{-1}$). Interestingly the DC conductivity and the electric activation energy are very close to the results of the similar glasses $(Ge_{28}Sb_{12}Se_{60})_{1-x}Ag_x$ studied by Bychkov et al.[38]. The changed trend of DC conductivity and electric activation energy E_a for a sample where x = 25 is probably caused by phase separation and by decreased content of silver in glassy part of sample, as mentioned before in section 3.1.

4.4.Radioactive tracer diffusion experiment

The temperature dependence of the diffusion coefficient deduced from the RTD experiment shows the Arrhenius behaviour. Measured RTD coefficients are comparable with calculated diffusion coefficients (Fig. 8). But there are differences in activation energies of the tracer diffusion experiment (E_d) and impedance measurement (E_a) as shown in Table 1. This results in dependency of Haven ratio on temperature. For the sample with 7.5 % at. of silver it is surprising that $D_{tracer} > D_\sigma$. This results in Haven ratio value higher than 1 (Haven ratio should be in range 0-1) [26, 27]. We do not know the origin of the discrepancy. We do repeat impedance measurement on newly prepared samples to exclude experimental error. The obtained results were the same. The RTD experiment gives reasonable data sets. The

measurement for each temperature gives a data set with coefficient of determination $R^2 \cong 0.98$.

5. Conclusion

The present study shows the way of silver incorporation into the chalcogenide glass $(GeS_2)_{50}(Sb_2S_3)_{50}$. Firstly, structural motifs in hosting matrix were described, and then reactants and products of interaction of hosting matrix with silver were identified. The structural motif of two interconnected pyramids $SbS_{3/2}$ is most likely the weakest part of the hosting matrix and is decomposed first. This is the first report to the author's knowledge that silver presence increases significantly the hardness of chalcogenide glass. The hardness is a macroscopic parameter and is dependent on the overall bonding strength between the constituting atoms of material. As was shown, the silver presence lowers the strength of bonds between the (Ge, Sb, S) atoms. Then increase of the hardness should origin elsewhere than in bonding strength. Most likely, the ability of the silver, to fills the cavities present in the glass, is responsible for the hardness increase. The performed impedance and RTD measurement shows that the studied material is an ionic conductor. Ionic conductivity increases with increase of silver content up to 8 orders of magnitude.

Author thanks to Sebastian Emmert and Tomas Netolicky for performing the part of measurement and to Ladislav Tichy, Jarda Bartak and Roman Svoboda for a fruitful discussion.

Authors appreciate financial support from the grants GAMA02/011 of TACR at University of Pardubice, LM2015082 and ED4.100/11.0251 from the Ministry of Education, Youth and Sports of the Czech Republic

[1] M. Frumar, B. Frumarova, T. Wagner, Amorphous and Glassy Semiconducting Chalcogenides, in: Comprehensive Semiconductor Science and Technology, 2011, pp. 206-261.

[2] M. Frumar, T. Wagner, Ag doped chalcogenide glasses and their applications, Current Opinion in Solid State and Materials Science, 7 (2003) 117-126.

[3] M. Ribes, E. Bychkov, A. Pradel, Ion Transport in Chalcogenide Glasses: Dynamics and Structural Studies, Journal of Optoelectronics and Advanced Materials, 3 (2001) 665-674.

[4] M. Kawasaki, J. Kawamura, Y. Nakamura, M. Aniya, Ionic conductivity of Agx(GeSe3)1-x (0≤x≤ 0.571) glasses, Solid State Ionics, 123 (1999) 259-269.

[5] R. Waser, Nanoelectronics and Information Technology, Wiley-VCH, 2012.

[6] L. Koudelka, M. Frumar, M. Pisárčik, Raman spectra of GeSbS system glasses in the S-rich region, Journal of Non-Crystalline Solids, 41 (1980) 171-178.

[7] C. Lin, Z. Li, L. Ying, Y. Xu, P. Zhang, S. Dai, T. Xu, Q. Nie, Network Structure in GeS_2–Sb_2S_3 Chalcogenide Glasses: Raman Spectroscopy and Phase Transformation Study, The Journal of Physical Chemistry C, 116 (2012) 5862-5867.

[8] L. Tichy, H. Ticha, On the "compositional threshold" in GeS_2-Sb_2S_3, $GeSe_2$-Sb_2Se_3 and GeS_2-Bi_2S_3 glasses, Materials Chemistry and Physics, 152 (2015) 1-3.

[9] R. Svoboda, J. Málek, M. Liška, Correlation between the structure and relaxation dynamics of $(GeS_2)_y(Sb_2S_3)_{1-y}$ glassy matrices, Journal of Non-Crystalline Solids, 479 (2018) 113-119.

[10] H. Tichá, M. Frumar, L. Tichý, A. Tříska, Relation between the temperature dependence of both the optical gap and the slope of the exponential absorption edge in glasses of the GeSbS system, Journal of Non-Crystalline Solids, 45 (1981) 437-440.

[11] J.W. Choi, Z. Han, B.-U. Sohn, G.F.R. Chen, C. Smith, L.C. Kimerling, K.A. Richardson, A.M. Agarwal, D.T.H. Tan, Nonlinear characterization of GeSbS chalcogenide glass waveguides, Scientific Reports, 6 (2016) 39234.

[12] L. Petit, N. Carlie, F. Adamietz, M. Couzi, V. Rodriguez, K.C. Richardson, Correlation between physical, optical and structural properties of sulfide glasses in the system Ge-Sb-S, Materials Chemistry and Physics, 97 (2006) 64-70.

[13] R. Shuker, R.W. Gammon, Raman-scattering selection-rule breaking and the density of states in amorphous materials, Physical Review Letters, 25 (1970) 222-225.

[14] D. Bletskan, I. Studenyak, V.V. Vakulchak, A.V. Lukach, Electronic structure of Ag_8GeS_6, Semiconductor physics quantum electronics & optoelectronics., 20 (2017) 19-25.

[15] R. Svoboda, M. Fraenkl, B. Frumarová, T. Wágner, J. Málek, Thermokinetic behaviour of Ag-doped $(GeS_2)_{50}(Sb_2S_3)_{50}$ glasses, Journal of Non-Crystalline Solids, 449 (2016) 12-19.

[16] L. Petit, N. Carlie, F. Adamietz, M. Couzi, V. Rodriguez, K.C. Richardson, Correlation between physical, optical and structural properties of sulfide glasses in the system Ge–Sb–S, Materials Chemistry and Physics, 97 (2006) 64-70.

[17] B. Frumarova, M. Frumar, J. Oswald, M. Kincl, M. Vlcek, Structure and optical properties of chalcohalide glasses doped with Pr^{3+} and Yb^{3+} ions, Journal of Non-Crystalline Solids, 355 (2009) 1865-1868.

[18] B. Frumarová, P. Němec, M. Frumar, J. Oswald, M. Vlček, Synthesis and optical properties of the Ge–Sb–S:$PrCl_3$ glass system, Journal of Non-Crystalline Solids, 256-257 (1999) 266-270.

[19] B. Minceva-Sukarova, M. Najdoski, I. Grozdanov, C.J. Chunnilall, Raman spectra of thin solid films of some metal sulfides, Journal of Molecular Structure, 410-411 (1997) 267-270.

[20] M. Balakrishnan, M.N. Kozicki, C.D. Poweleit, S. Bhagat, T.L. Alford, M. Mitkova, Crystallization effects in annealed thin GeS_2 films photodiffused with Ag, Journal of Non-Crystalline Solids, 353 (2007) 1454-1459.

[21] E.I. Kamitsos, J.A. Kapoutsis, G.D. Chryssikos, G. Taillades, A. Pradel, M. Ribes, Structure and Optical Conductivity of Silver Thiogermanate Glasses, Journal of Solid State Chemistry, 112 (1994) 255-261.

[22] M. Mitkova, M.N. Kozicki, Ag-photodoping in Ge-chalcogenide amorphous thin films—Reaction products and their characterization, Journal of Physics and Chemistry of Solids, 68 (2007) 866-872.

[23] C.D. Jeppe, M. Philipp, R. Bernhard, L.S. David, Fundamental questions relating to ion conduction in disordered solids, Reports on Progress in Physics, 72 (2009) 046501.

[24] J.C. Dyre, The random free-energy barrier model for ac conduction in disordered solids, J Appl Phys, 64 (1988) 2456-2468.

[25] D.S. Patil, K. Shimakawa, V. Zima, T. Wagner, Quantitative impedance analysis of solid ionic conductors: Effects of electrode polarization, J Appl Phys, 115 (2014) 143707.

[26] J.O. Isard, The Haven ratio in glasses, Journal of Non-Crystalline Solids, 246 (1999) 16-26.

[27] R. Terai, R. Hayami, Ionic diffusion in glasses, Journal of Non-Crystalline Solids, 18 (1975) 217-264.

[28] A. Feltz, Amorphous inorganic materials and glasses / Adalbert Feltz, 2018.

[29] R. Vahalová, L. Tichý, M. Vlček, H. Tichá, Far infrared spectra and bonding arrangement in some Ge-Sb-S glasses, Physica Status Solidi (A) Applied Research, 181 (2000) 199-209.

[30] M.M. Smedskjaer, J.C. Mauro, Y. Yue, Prediction of Glass Hardness Using Temperature-Dependent Constraint Theory, Physical Review Letters, 105 (2010) 115503.

[31] J.-P. Guin, T. Rouxel, V. Keryvin, J.-C. Sanglebœuf, I. Serre, J. Lucas, Indentation creep of Ge–Se chalcogenide glasses below Tg: elastic recovery and non-Newtonian flow, Journal of Non-Crystalline Solids, 298 (2002) 260-269.

[32] C.T. Hach, K. Cerqua-Richardson, J.R. Varner, W.C. LaCourse, Density and microhardness of As–Se glasses and glass fibers, Journal of Non-Crystalline Solids, 209 (1997) 159-165.

[33] J. Akola, B. Beuneu, R.O. Jones, P. Jóvári, I. Kaban, J. Kolář, I. Voleská, T. Wágner, Structure of amorphous Ag/Ge/S alloys: Experimentally constrained density functional study, Journal of Physics Condensed Matter, 27 (2015) 485304.

[34] J. Akola, P. Jóvári, I. Kaban, I. Voleská, J. Kolář, T. Wágner, R.O. Jones, Structure, electronic, and vibrational properties of amorphous AsS_2 and $AgAsS_2$: Experimentally constrained density functional study, Physical Review B - Condensed Matter and Materials Physics, 89 (2014) 485304.

[35] L. Calvez, Transparent chalcogenide glass-ceramics, in: Chalcogenide Glasses, 2013, pp. 329.

[36] S. Stehlik, J. Kolar, H. Haneda, I. Sakaguchi, M. Frumar, T. Wagner, Phase Separation in Chalcogenide Glasses: The System AgAsSSe, Int. J. Appl. Glass Sci., 2 (2011) 301-307.

[37] A. Pradel, M. Ribes, Ionic conductivity of chalcogenide glasses, in: Chalcogenide Glasses, 2013, pp. 169-208.

[38] E. Bychkov, V. Tsegelnik, Y. Vlasov, A. Pradel, M. Ribes, Percolation transition in Ag-doped germanium chalcogenide-based glasses: Conductivity and silver diffusion results, Journal of Non-Crystalline Solids, 208 (1996) 1-20.

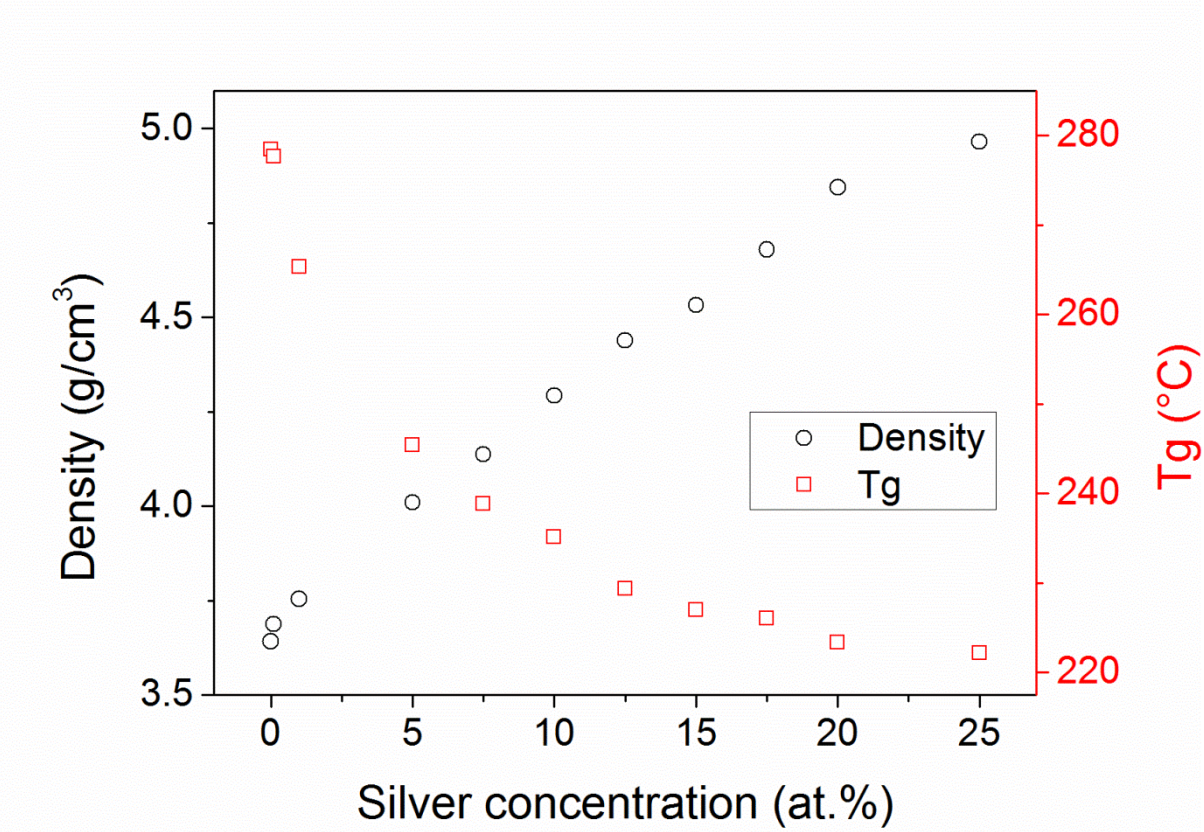

Fig. 1. Density and glass-transition temperature of the $Ag_x((GeS_2)_{50}(Sb_2S_3)_{50})_{1-x}$.

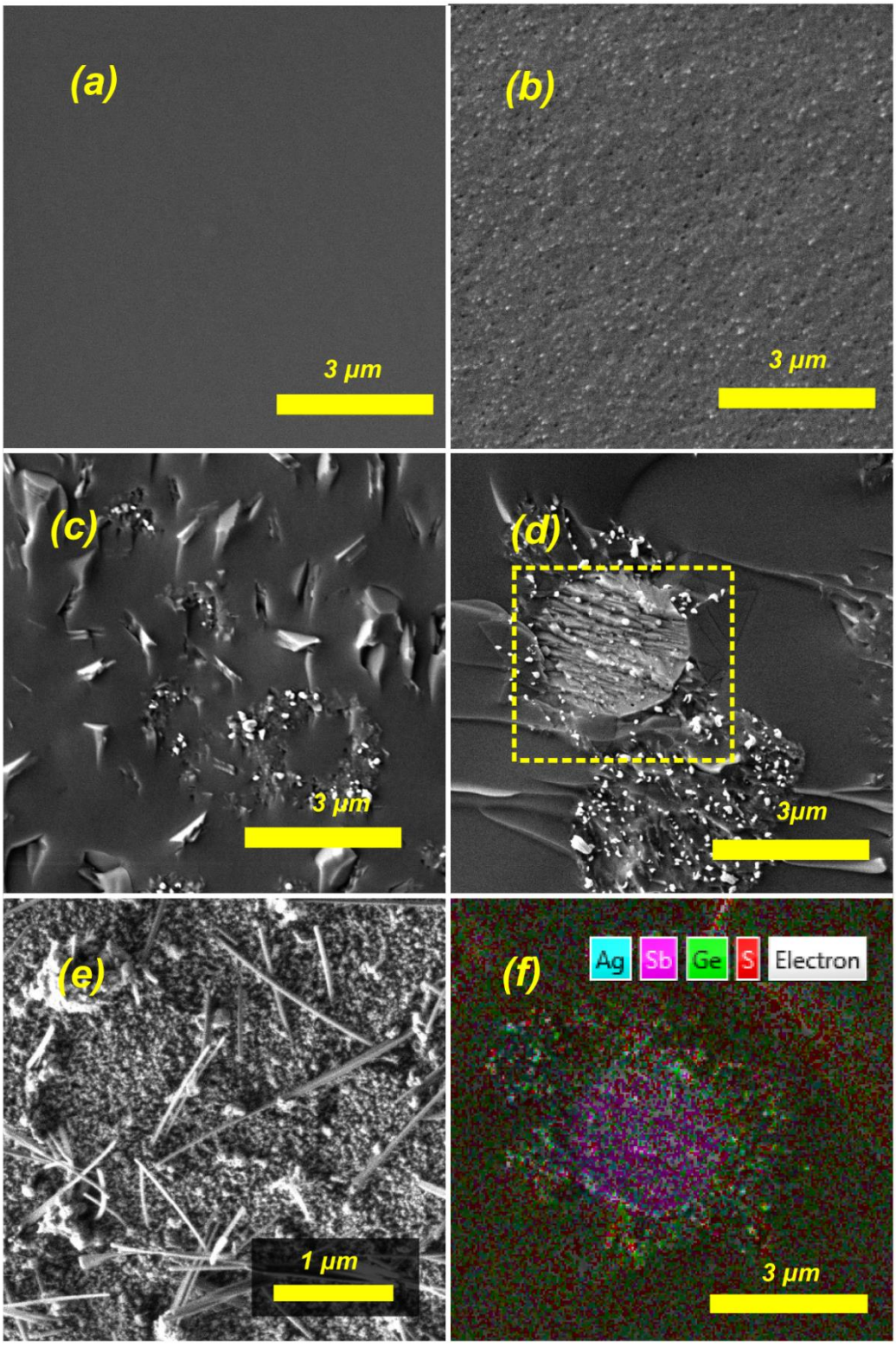

Fig. 2. a-f) SEM images of samples $Ag_x((GeS_2)_{50}(Sb_2S_3)_{50})_{1-x}$ a) x = 15 glass without a crystals, b) x = 17.5 with antimony crystals , c) x = 20 with antimony crystals d) x = 25 phase separated antimony

sphere is visible e) x = 20 after wet etch in NaOH solution with needle like antimony crystals 1-2 microns in length, f) x = 25, EDX mapping identifies antimony sphere

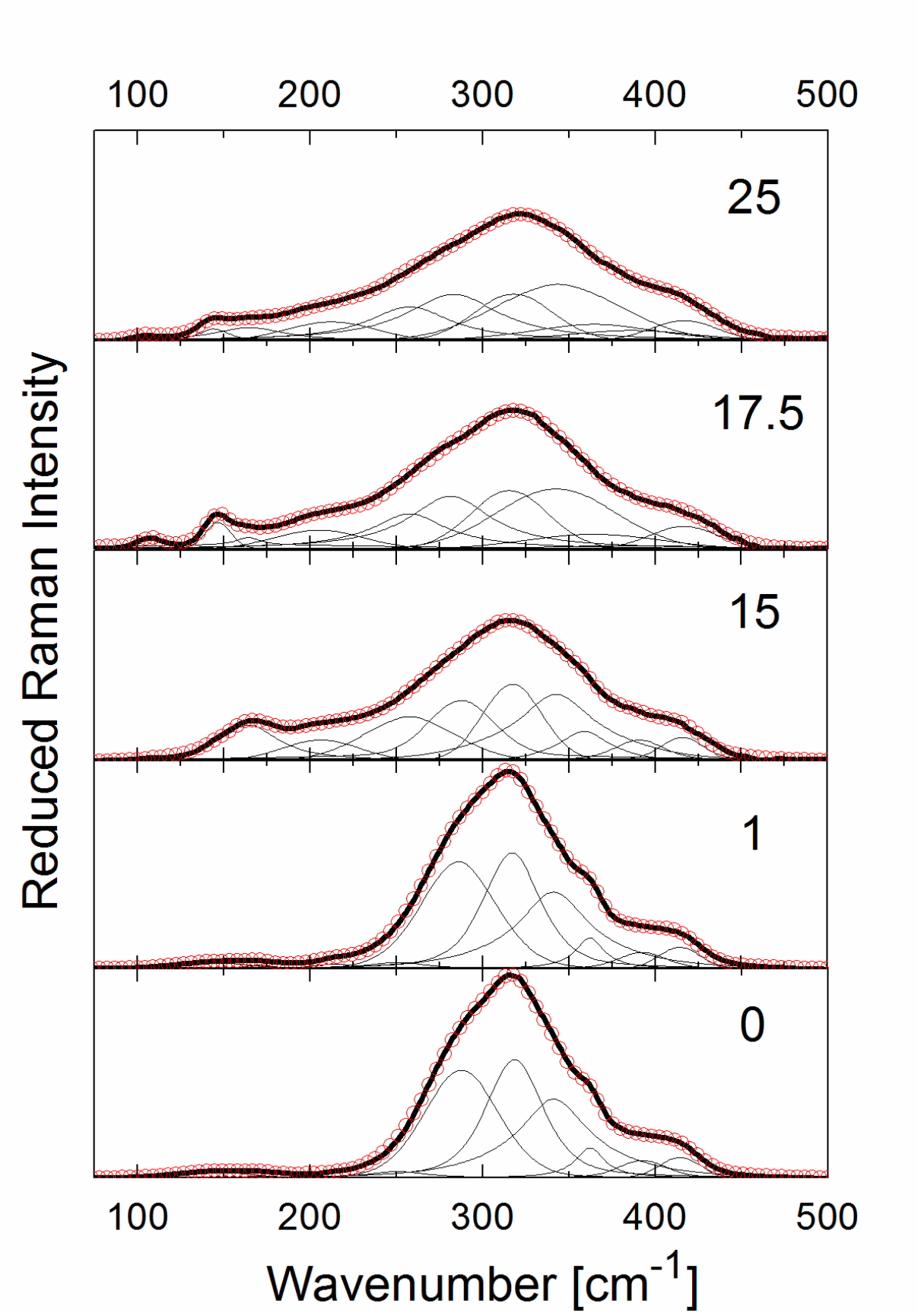

Fig. 3. Decomposed Raman spectra of $Ag_x((GeS_2)_{50}(Sb_2S_3)_{50})_{1-x}$ for silver concentration 0, 1, 15, 17.5, and 25 at.%

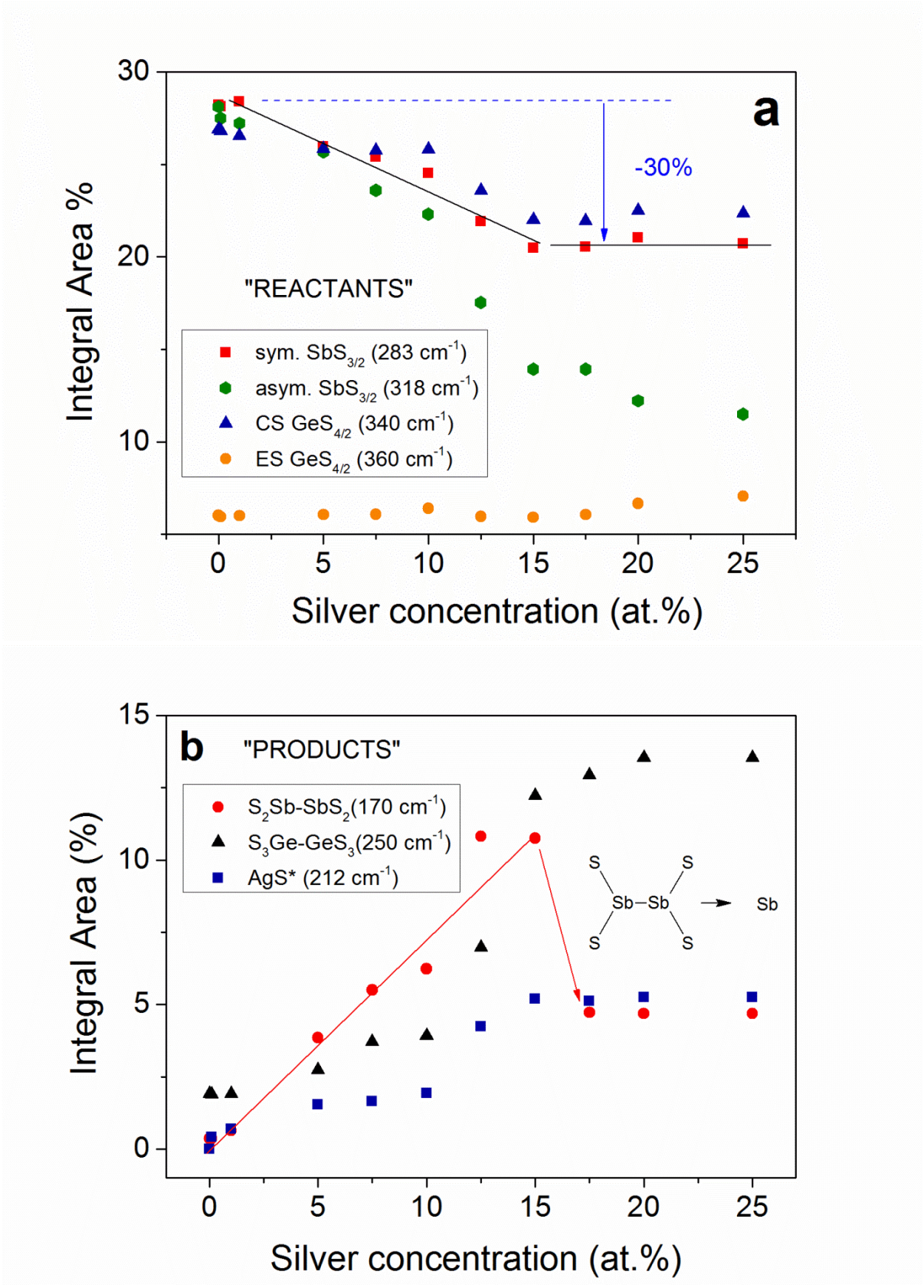

Fig. 4. a) and b) integrated intensities of decomposed Raman peaks corresponding to particular vibration normalized with respect to the overall integral area. a) “REACTANTS” are units identified by Raman spectroscopy corresponding to the structural motifs in the hosting matrix, B) “PRODUCTS” are newly created structural motifs by reaction with silver. Lines were used as a guide of eye.

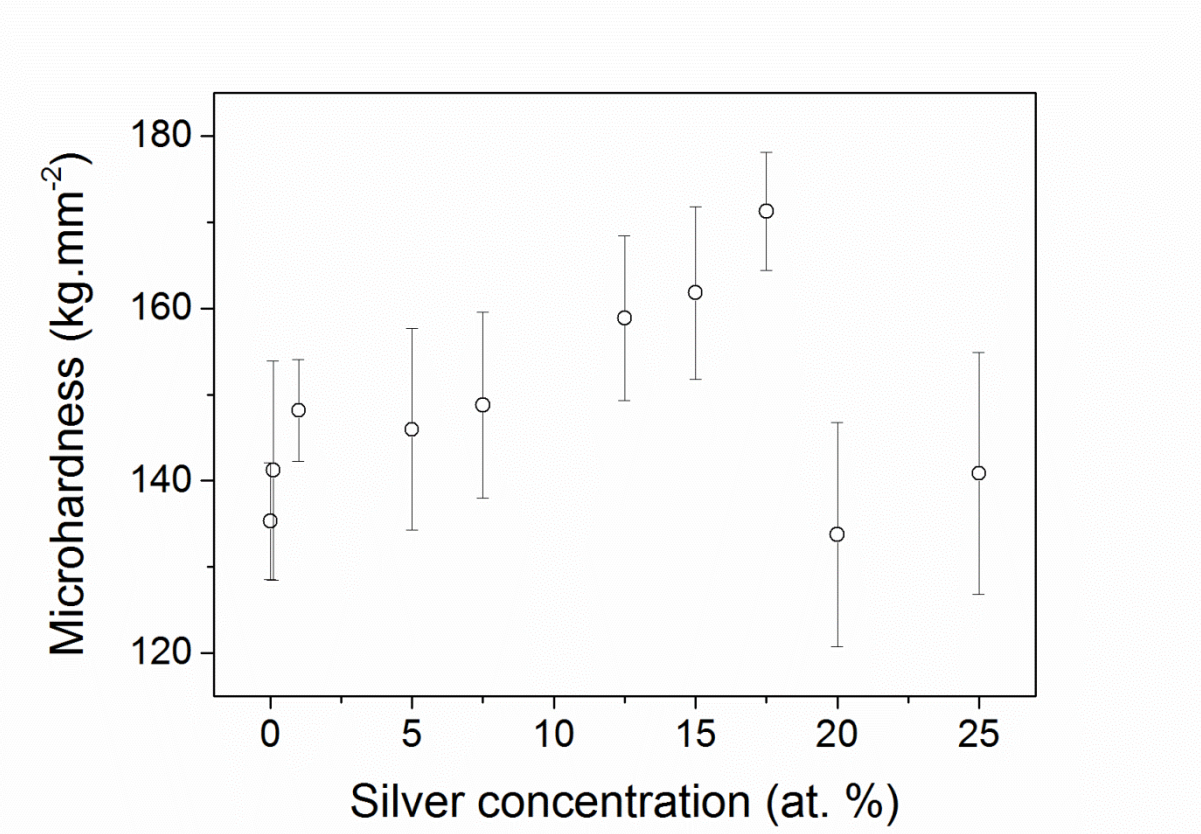

Fig. 5. Microhardness of the $Ag_x((GeS_2)_{50}(Sb_2S_3)_{50})_{1-x}$ samples. Hardness increases up to 26 % (x = 17.5).

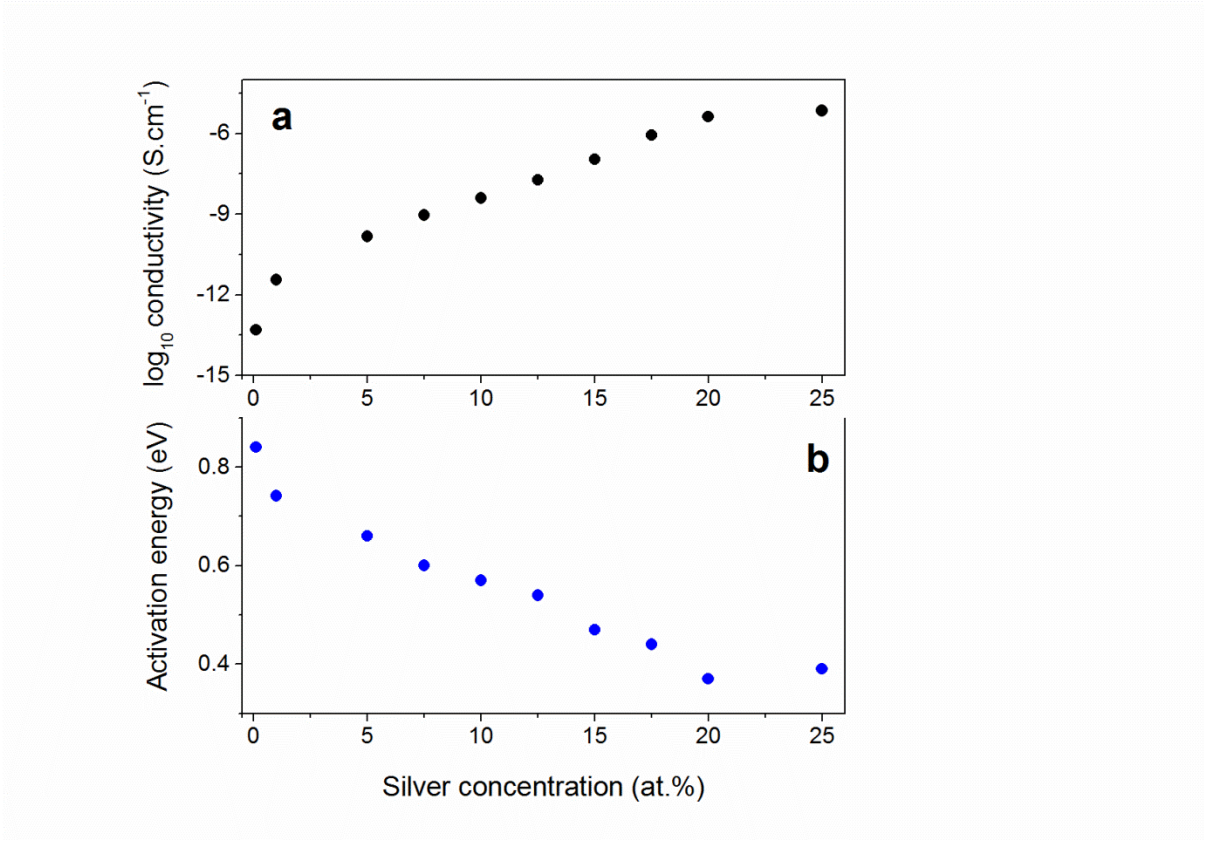

Fig. 6. a) DC conductivity and b) electric activation energy of $Ag_x((GeS_2)_{50}(Sb_2S_3)_{50})_{1-x}$ at 293 K (for x = 0.1 - 25).

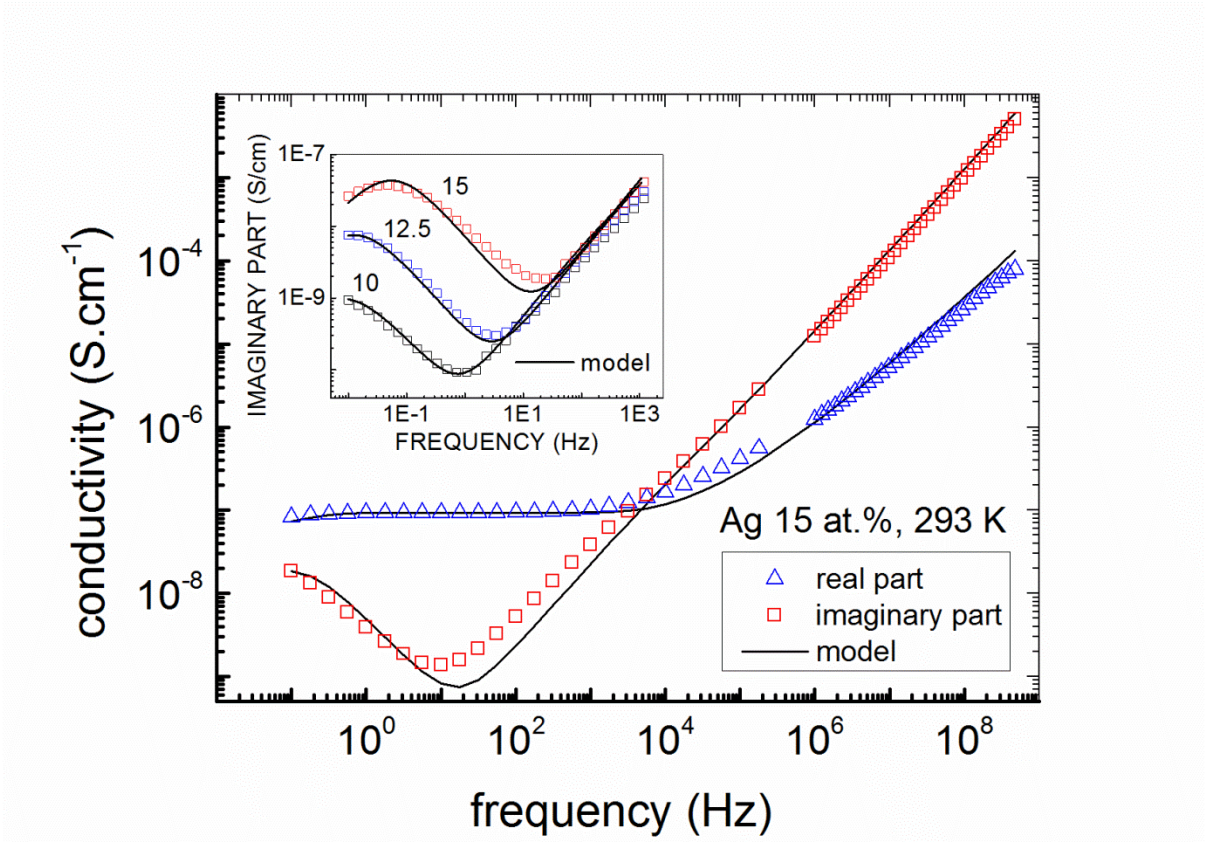

Fig. 7. Impedance spectra of the sample with 15 at. % of silver at 293 K. Model curve is based on equations (1-3) . Inset shows the electrode polarization effect of the samples where x = 10, 12.5, and 15 at 293 K.

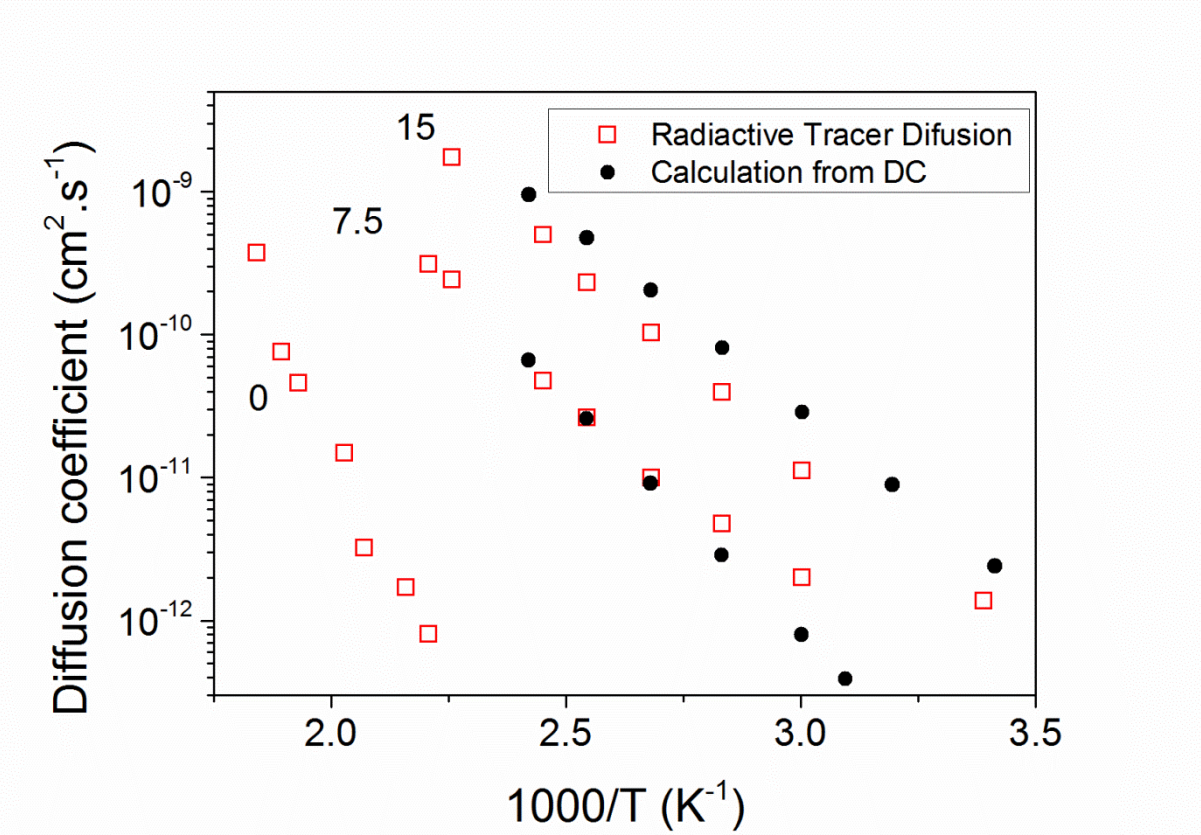

Fig. 8. The comparison of the diffusion coefficients. 1st obtained by Radioactive Tracer Diffusion experiment and 2nd by calculation from DC conductivity.

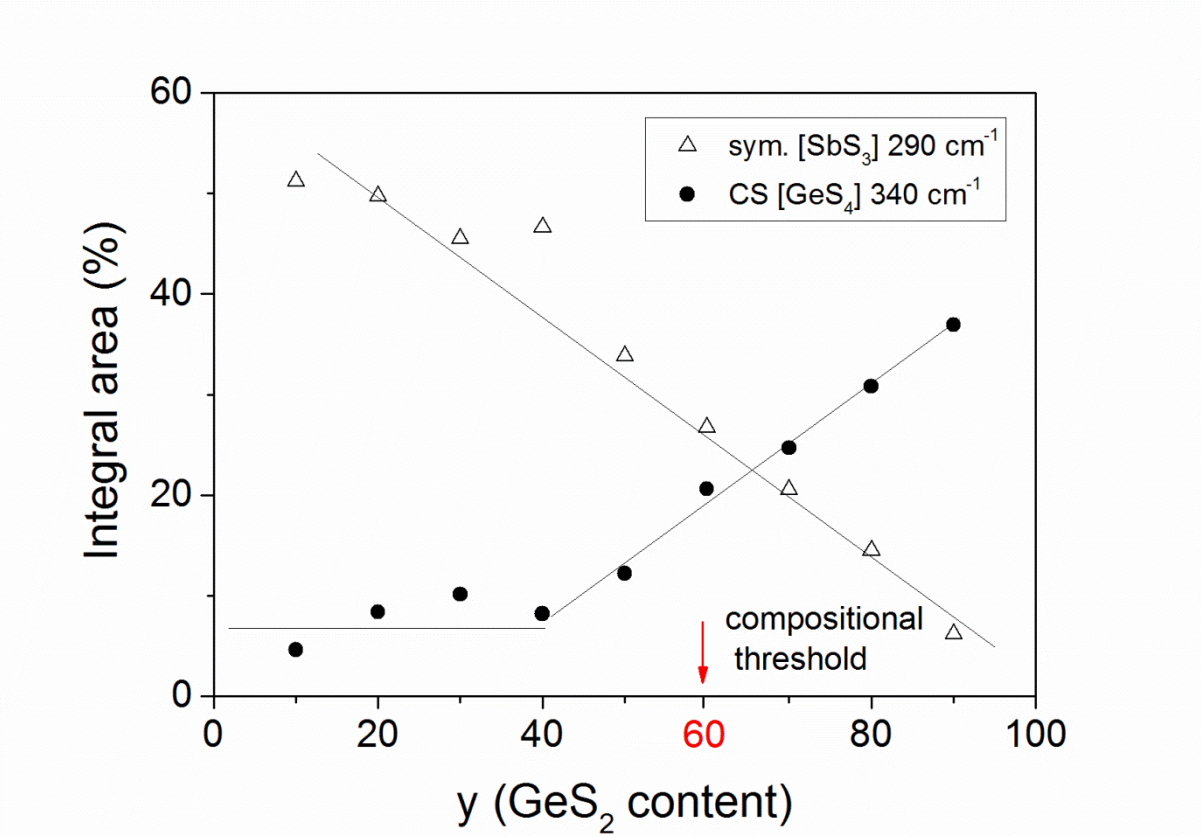

Fig. 9. Data taken over from R. Svoboda et al. show integrated intensities of deconvoluted Raman peaks in the system $(GeS_2)_y(Sb_2S_3)_{1-y}$. Data are normalized with respect to the overall integral area. The signal of CS $GeS_{4/2}$ minimizes for $y < 60$ when compositional threshold is reached. The signal of symmetrical vibration $SbS_{3/2}$ pyramid is proportional to the content of Sb_2S_3.

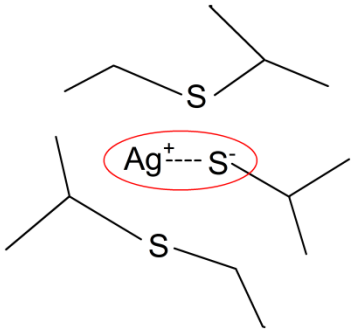

Fig. 10. Structure detail shows the silver bonded by ionic bond with sulphur. Silver terminates the structural chain.